


Article

Selective Laser Melting of (Fe-Si-B)/Cu Composite: Structure and Magnetic Properties Study

Danil Erutin, Anatoly Popovich and Vadim Sufiiarov * 

Institute of Mechanical Engineering, Materials, and Transport, Peter the Great St. Petersburg Polytechnic University, 195251 St. Petersburg, Russia

* Correspondence: vadim.spbstu@yandex.ru

Abstract: A mixture of original 1CP powder and 10 wt.% of pure Cu-powder was prepared and 1CP-Cu composite samples were obtained by selective laser melting using different process parameters. Comparison of pure 1CP and composite samples showed that addition of Cu halved the porosity percentage of the obtained material. Distribution of Cu-phase in 1CP-matrix can be recognized as uniform in all the samples. X-ray diffraction of samples showed the presence of α -Fe solid solution, iron boride Fe_2B , and crystal Cu. Scanning electron microscopy analysis also allowed to discover ordered solid solution Fe_3Si in samples microstructure. Differential scanning calorimetry data showed that composite sample contains amorphous phase as opposed to pure 1CP sample manufactured using the same process parameters. Magnetic properties of samples were studied, and it was found that addition of 10 wt.% of Cu allowed to reduce magnetic field energy losses by approximately four times.

Keywords: additive manufacturing; selective laser melting; bulk metallic glass; magnetic properties



Citation: Erutin, D.; Popovich, A.; Sufiiarov, V. Selective Laser Melting of (Fe-Si-B)/Cu Composite: Structure and Magnetic Properties Study. *Metals* **2023**, *13*, 428. <https://doi.org/10.3390/met13020428>

Academic Editors: Hany Hassanin, Leszek Adam Dobrzanski, Yung C. Shin and Lai-Chang Zhang

Received: 17 January 2023

Revised: 10 February 2023

Accepted: 15 February 2023

Published: 19 February 2023



Copyright: © 2023 by the authors. Licensee MDPI, Basel, Switzerland. This article is an open access article distributed under the terms and conditions of the Creative Commons Attribution (CC BY) license (<https://creativecommons.org/licenses/by/4.0/>).

1. Introduction

Soft magnetic materials development is a key in case of increasing the electric engines efficiency, which is a very important challenge in a rapidly developing market worldwide. Fe-based nanocrystalline alloys and bulk metallic glasses (BMGs) are some of the most prospective soft-magnetic materials nowadays due to the fascinating electric and magnetic properties [1,2]. Bulk metallic glasses or amorphous metallic materials are a type of solid materials in which there is no long-range order in the atomic arrangement. Such state of the material can be achieved with high cooling rates from the liquid state due to the fixation of atoms in its initial positions, which they occupy in the melt. An amorphous metallic material (metallic glass) does not have a crystalline lattice and crystalline defects, which is why there is no mechanical and magnetic properties anisotropy. Metallic glasses based on ferromagnetic alloys exhibit better soft magnetic properties than crystalline ferromagnetic materials, such as lower coercivity, higher values of saturation magnetization, higher magnetic permeability, and electrical resistivity. Due to the higher level of soft magnetic properties of metallic ferromagnetic glasses, their use as a magnetic core material of an electromagnetic device allows increasing its efficiency by significantly reducing the magnetic field energy losses for remagnetization and eddy currents [1].

Currently, such methods as direct casting [3,4] and thermoplastic forming [5–12] are widely used in industrial manufacturing of Fe-based BMGs, but there are a lot of restrictions related to detail's geometry and material's glass forming ability, which can be overcome by using selective laser melting (SLM) technology based on powder bed fusion additive manufacturing process [13–15]. Layer-by-layer melting of powder layers of 20–60 μm makes it possible to achieve cooling rates up to 10^{6-8} K/s and this circumstance is an excellent opportunity to use SLM for producing BMGs of complex geometric configuration. However, it is very difficult to obtain defect-free Fe-based material structure without any

defects via SLM due to extremely high levels of internal stresses and technological features of the process [16–23]. There are different ways that scientists are using to improve the selective laser melted amorphous and nanocrystalline samples quality, such as optimal process parameters selection and application of multi-scanning strategies with different patterns. Using these approaches allows to significantly improve the sample's quality but mostly not to fully exceed the internal stress influence, which is a negative factor for targeted magnetic and mechanical properties isotropy. In addition to the quality of the samples, degree of amorphization of the resulting material is also one of the most important factors in case of obtaining bulk metallic glasses. Obtaining a material with a minimal degree of crystallinity involves the suppression of crystallization both when cooling the molten metal and when absorbing the heat of the melt by the already solidified part of the product [1].

Authors of [17] used a double scanning strategy with KUAMET6B2 Fe-based powder ($\text{Fe}_{73.7}\text{Si}_{11}\text{B}_{11}\text{C}_2\text{Cr}_{2.28}$). Obtained samples analysis allowed to conclude that double scan strategy is advantageous for densification and for enhancing saturation magnetization. Double scan increased the time of powder contact with laser beam; increased exposure led to shrinkage of voids, and density of the samples dramatically increased. Double scanning combined with high volume energy density can lead to very high density of 96% and corresponding saturation magnetization of 1.22 T. More importantly, double scanning induces reflow in the melt pool, securing compositional uniformity. Using of such approach enhanced amorphization degree of the samples to a level as high as 47%. As a consequence, coercivity of the samples significantly decreased.

Another scientific group developed more complex scanning strategy in their research [21]. Authors used a “point-random” scanning strategy to obtain amorphous samples with decent magnetic properties from KUAMET52 powder ($\text{Fe}_{71}\text{Si}_{10}\text{B}_{11}\text{C}_6\text{Cr}_2$) via selective laser melting. Mentioned scanning strategy consists in dividing the powder layer into quadrants and successively melting a random section of the layer so that each successive melting zone is not in the same quadrant as the previous one. The main idea of such approach was the impact reduction of the secondary heating of solidified zones. Single melted samples, obtained by the mentioned researchers, showed poor amorphization with well-separated amorphous regions and coercivity of 1032 A/m. Second melting increased the amorphous phase content by over an order of magnitude-up to 89.6% and reduced coercivity over four times to 238 A/m. X-ray diffraction analysis showed significant difference between, arising from melt, disordered Fe(Si) phase and devitrified, ordered Fe_3Si . Coexistence of those phases has been shown in heat affected zone by electron diffraction. Beneficial effect of the novel remelting strategy has been explained on the basis of restricted crystallization in heat-affected zone and reduction of sample overheating, by application of the “point-random” scanning strategy.

One of the possible ways for further improvement of Fe-based selective laser melted alloy's quality is addition of more fusible element or multi-element powder to initial powder material. The main idea of this approach consists in filling of the matrix material cracks by the fusible secondary phase. Moreover, secondary material can intensify the matrix cooling by partially absorbing of the incoming heat and may influence matrix material glass-forming ability by diffusion, which can contribute to amorphization. In addition to the possibilities of the outlined approach, using the secondary element powder in conjunction with the selective laser melting parameters and scanning strategy optimization may allow to obtain material with the gradient structure, which theoretically can outperform the conventionally accepted ones.

Using Cu powder with initial Fe-based alloy powder in SLM allowed the authors of [19] to obtain crack-free composite microstructure with uniform distributed crystal phase Cu and amorphous FeCrMoCB BMG. However, crack-free microstructure was obtained in composite with 40 vol. % of Cu. Authors have not investigated the magnetic properties of the obtained material but such concentration of non-ferromagnetic element with low

electrical resistivity cannot provide a decent level of soft-magnetic properties due to low integral volume of magnetic domain-containing material and to high eddy current losses.

Ni can also inhibit the crystallization of Fe-based material in the powder bed fusion process. Authors of [24] studied the effect of Ni addition to the Fe₅₀Cu₅₀ composition on the material crystallization mechanism through the mathematical simulation of the selective laser melting process. It was figured out that without the addition of Ni, the populations of Cu-centered and Fe-centered icosahedral polyhedrons (geometric configuration of atoms in the amorphous phase) are extremely small, while the Ni-centered icosahedral polyhedron is zero. By increasing the content of Ni, an obvious and monotonic increment is observed both in Ni-centered and Fe-centered icosahedral polyhedrons, while Cu-centered icosahedral polyhedrons first indicate an increment and then a decrease with further increasing Ni content from 20.0%, which is uncoordinated with the increasing Ni content. The full volume of the data obtained by the authors allows conclusions to be drawn that high Ni content can inhibit the nucleation and growth of crystals while increasing the fraction of the amorphous phase. However, the melting point of Ni is very close to that of Fe. This feature of Ni does not allow for crack filling effect in SLM of composite with Fe-based alloy, which was partially demonstrated by the mentioned researchers [23].

Analysis of the abovementioned papers and studies made it clear that addition of Cu to the Fe-based powder allows to obtain better quality samples via selective laser melting. Both scientific groups used significant amounts of Cu, which is a barrier to obtaining good magnetic characteristics. It was decided to add a smaller amount of fine Cu powder to the FeSiB alloy powder and investigate the magnetic properties of obtained material.

In the present work, 1CP amorphous-nanocrystalline FeSiB alloy was selected to obtain a composite material with Cu via SLM. The aim of the present work was to investigate the microstructure, phase composition, and magnetic properties of the composite obtained with different SLM parameters and to compare this data to that of the selective laser-melted 1CP to find out how addition of Cu affects density, amorphization degree, and magnetic properties of the material.

2. Materials and Methods

Initial powders of 1CP [1] and copper were used in the presented study. Mixture of gas-atomized [25] 1CP powder (spherical particles) with mean particle size of 41.8 μm and 10 wt.% of copper powder (particles with dendrite morphology) with mean particle size of 26.9 μm was prepared by blending the powders in a gravitational mixer for 24 h (Figure 1).

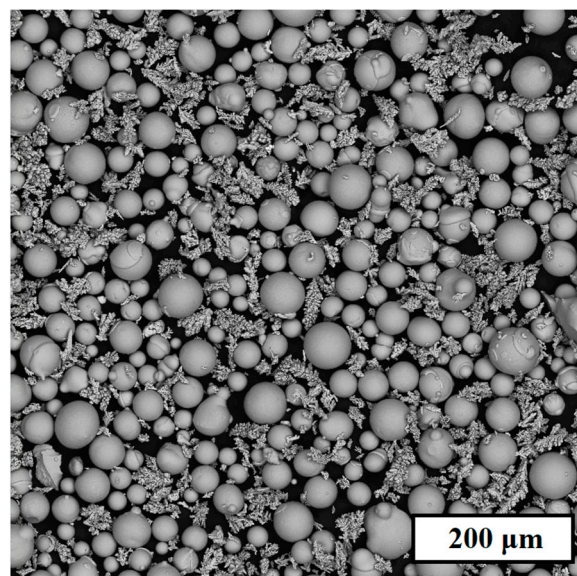


Figure 1. Mixture of the initial 1CP and copper powders after blending in 24 h.

Apparent density measurements were made by pouring the powder mixture into a funnel from which it flowed into a 25 cm³ cup. After filling the cup, the funnel was moved away, and excess powder was smoothed out with a trowel. Apparent density was determined by weighing the powder in the cup in grams and dividing by 25 cm³ and the value is 3.97 g/cm³.

The particle size distribution of the powder was determined by laser diffraction on the Analysette 22 NanoTec plus (Fritsch GmbH, Idar-Oberstein, Germany) with a total measuring range of 0.01–2000 µm. Mean value of the particle size of the mixture is 41.2 µm.

The macrostructure of the samples was studied using a Leica DMI5000 optical microscope. Image analysis was performed with ImageJ program.

The microstructure of the powder and the obtained samples were studied using a Tescan Mira3 LMU (TESCAN ORSAY HOLDING, Brno, Czech Republic) scanning electron microscope (SEM). The etching of the samples was carried out in a 25% nitric acid solution in water.

Temperatures of phase transitions were studied using differential scanning calorimeter (DSC) Q2000 (TA Instruments, New Castle, DE, USA) equipped with automatic sampler, RCS90 cooling system and T-zero baseline alignment technology. Samples were heated in an argon flow to a temperature of 900 °C at a heating rate of 20 °C/minute followed by a second heating of the cooled samples to the same temperature. Figure 2 shows the differential scanning calorimetry results of the 1CP powder material presented by two curves: the red curve for the primary heating of the original material and the blue one for the secondary heating of the material (cooled down after primary heating).

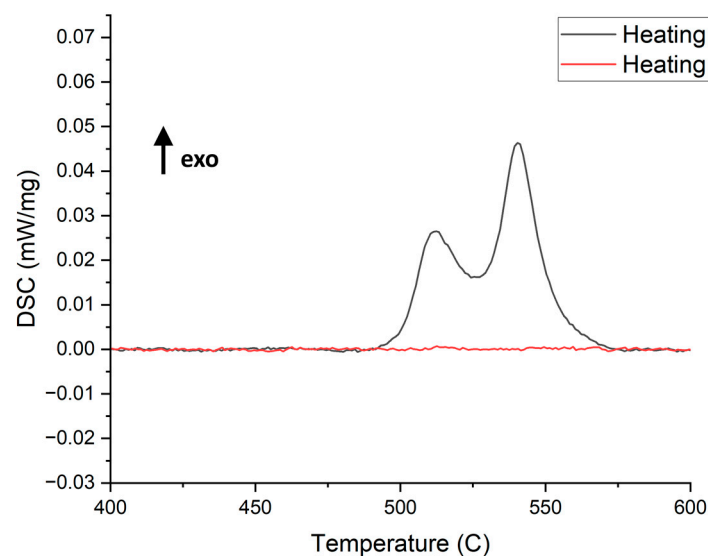


Figure 2. DSC heating curves for initial 1CP powder.

The primary heating curve shows peaks indicating a phase transformation during heating. This process occurs for 1CP alloy powder in the temperature range from 450 to 575 °C. The absence of the secondary heating peaks shows the accordance of the peaks to crystallization process. Based on the differential scanning calorimetry data it could be concluded that heating above 450 °C would lead to the beginning of crystallization processes of amorphous phase in case of presence of amorphous phase in the samples during heat treatment of samples obtained from this powder. 1CP powder also was investigated with transmission electron microscope in our previous work [1] and it was found that it is not fully amorphous, which makes it impossible to determine the exact degree of amorphization of the samples obtained using differential scanning calorimetry data, but the value obtained for 1CP powder (amorphous phase crystallization enthalpy of 4353 J/g) can be used for comparison purposes.

The phase composition was analyzed with a Bruker D8 Advance (Bruker Corp., Billerica, MA, USA) X-ray diffractometer (XRD) using Cu K α ($1\frac{1}{4}$ 1.5418 Å) irradiation.

The magnetic hysteresis loops for the samples were measured by Lake Shore 7410 vibration sample magnetometer (VSM) (Lake Shore Cryotronics, Westerville, OH, USA) at room temperature (22 °C) and under applied different magnetic fields from $-18,000$ to $+18,000$ Oe.

Samples were manufactured using SLM280HL (SLM Solutions GmbH, Lübeck, Germany) selective laser melting system with YLR-Laser with a wavelength of 1070 μm and focus size of 80 μm in a nitrogen atmosphere. All the samples for investigation were prepared in the same conditions.

3. Results

Four samples of elliptical prism geometry ($5 \times 10 \times 5 \text{ mm}^3$) were successfully manufactured by selective laser melting in a nitrogen atmosphere: sample 1 was made of 1CP powder and the other samples (2–4) were made of mixture of 1CP powder with copper. Preliminary tests were performed to define the most suitable SLM parameter sets [1]. Parameters applied for selective laser melting fabrication are presented in Table 1.

Table 1. Parameters applied for selective laser melting samples fabrication.

Sample Number	Laser Power (W)	Laser Scanning Speed (mm/s)	Hatch Distance (mm)	Layer Thickness (mm)
1	90	1200	0.12	0.02
2	90	1200	0.12	0.02
3	90	1200	0.08	0.02
4	90	1200	0.05	0.02

Optical microscope images of the obtained samples are presented in Figure 3.

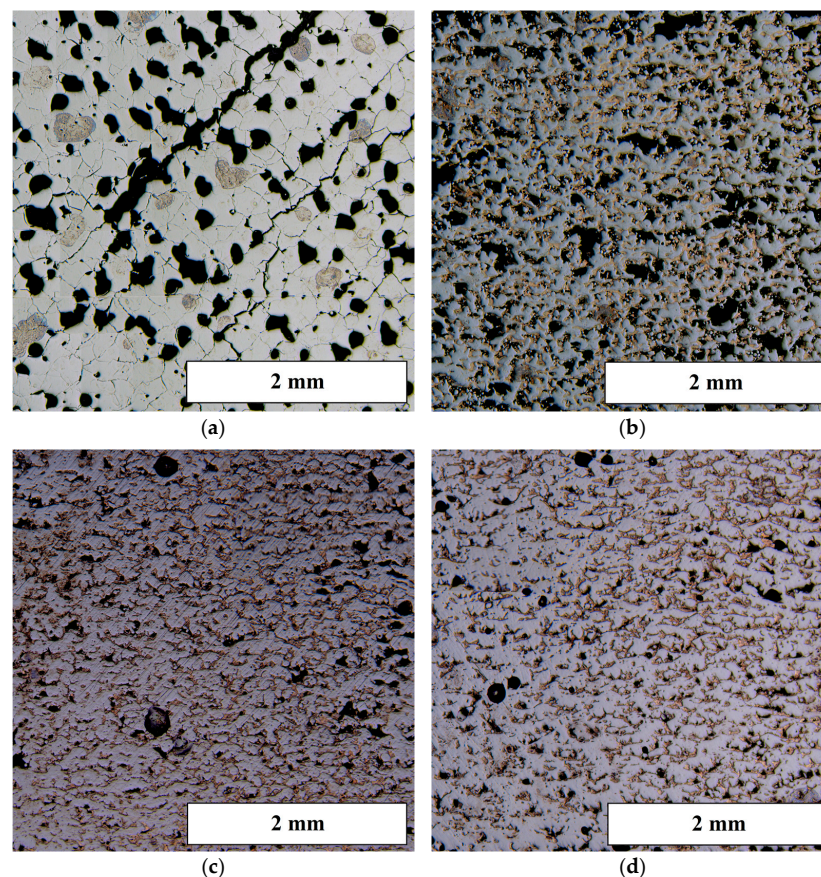


Figure 3. Macrostructure of the samples 1–4 (a–d).

Obtained images shows that macro-cracks observable in 1CP sample are almost entirely absent in 1CP sample with Cu obtained with the same selective laser melting parameters and also in the other 1CP samples with Cu. However, all the samples contain different number of loose spots through the presence of pores. Porosity assessment results were obtained with the image analysis and are presented in Table 2.

Table 2. Porosity percentage data obtained from samples.

Sample	Porosity (%)
1	27.03 ± 0.31
2	13.69 ± 0.54
3	4.36 ± 0.13
4	4.94 ± 0.21

Porosity data testifies that the addition of Cu led to a reduction in the porosity percentage by about half, from 27.03% to 13.69%. Regarding the samples containing Cu, there is a significant decrease in porosity with a decrease in hatch distance parameter from 0.12 mm to 0.08 mm, which is 68%. However, further decrease to 0.05 resulted in slightly increased porosity percentage: from 4.36% to 4.94%.

Increased hatch distance value (relative to 0.08 mm) led to decreased volume energy density not enough to form a dense metal: multiple single pores formed many clusters, which is clearly visible in Figure 3b. Decreased hatch distance value led to higher volume energy density, which may have led to amplified spattering on each new layer surface and formation of the recoating defects [25]. Presence of the heat retentive Cu in the powder layer contributed to the enhancement of the increased hatch distance effect due to the higher energy requirement for the material to be dense; however, regarding the hatch distance decreasing effect, presence of Cu might partially de-intensify spattering of the liquid metal, which explains the difference in the porosity percentage change with almost the same change in hatch distance parameter. Macro distribution of Cu in samples was examined with optical microscope and image processing: Cu phase distribution can be recognized as even in all the samples. It is clearly visible that Cu phase precipitations have a form of quasi continuous net in samples 2 and 3, which cannot be said about sample 4 (Figure 4).

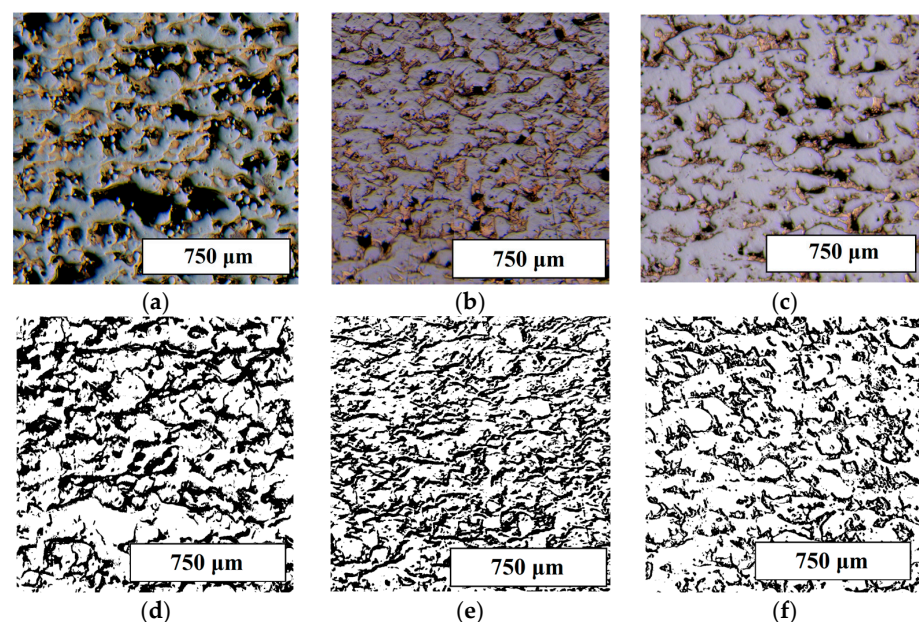


Figure 4. Enlarged regions of samples 2–4 (a–c). Cu macro-distribution in the same regions of samples 2–4 (d–f); the black color indicates Cu-phase.

Phase composition of the samples was revealed by X-ray diffraction (Figure 5).

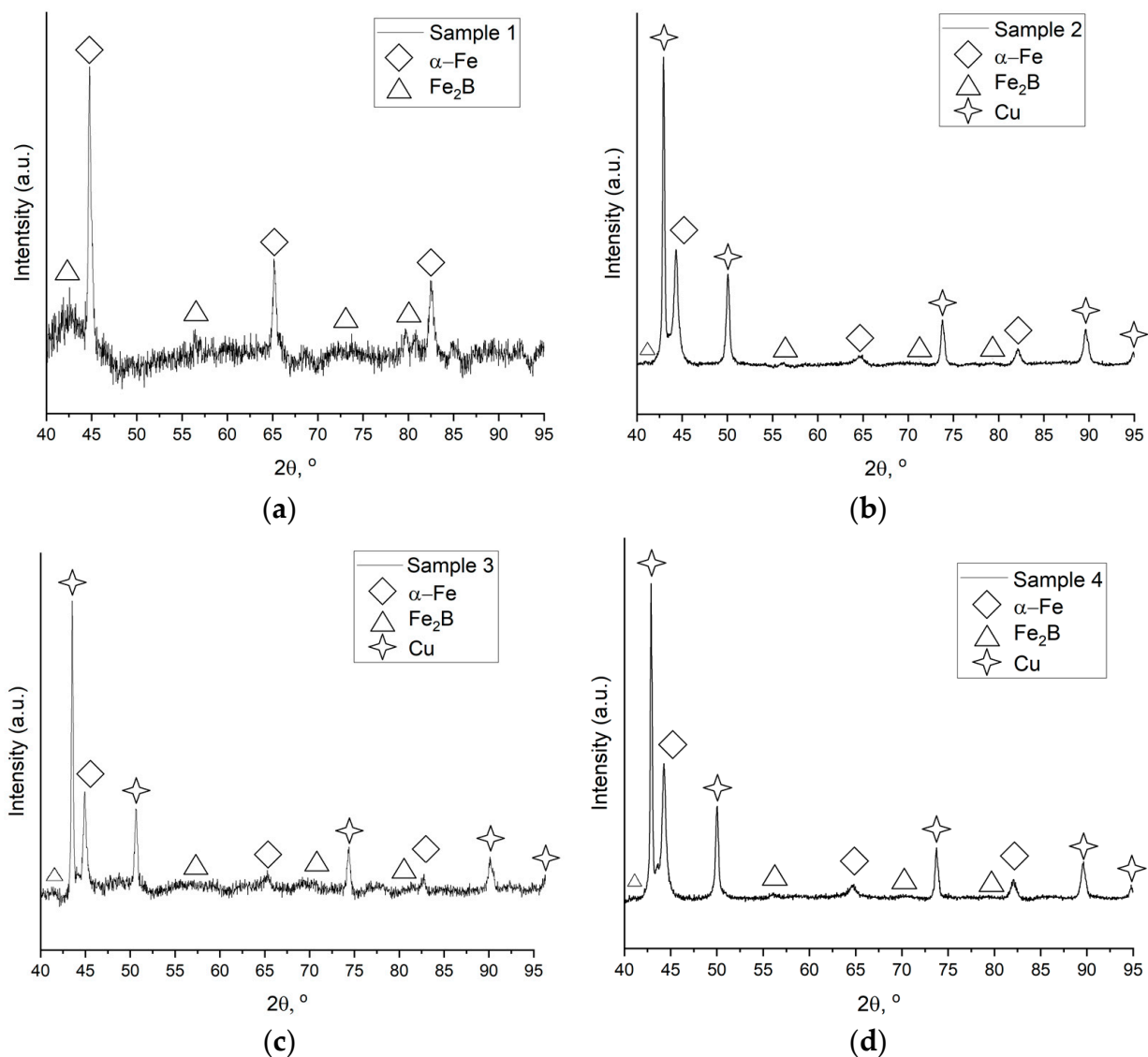


Figure 5. X-ray diffraction patterns of the samples 1–4 (a–d).

Phase composition of all the samples is characterized by the presence of the α -Fe solid solution (Im-3 m space group) and iron boride Fe_2B (I4/mcm space group). Revealed phases are typical for selective laser melted alloys of Fe-Si-B system [1,2,26]: α -Fe (Si) solid solution is formed in the cooling process and iron boride Fe_2B is emitted by the secondary heating of the cooled regions. A similar selective laser-melted alloy has been analyzed in depth by X-ray analysis in [27]. Diffraction patterns of the samples of 1CP with Cu composition also contains peaks related to Cu. Significant size of Cu peaks relative to highest α -Fe peaks in composite samples is connected to high concentration of Cu on the surface of the samples pieces subjected to X-ray analysis.

Absence of the halo on the diffraction patterns attests to the smallness of the amorphous phase content in all the samples. Amorphous phase crystallization enthalpy of the samples was examined with differential scanning calorimetry (Figure 6), numerical data for the 1CP matrix are presented in Table 3.

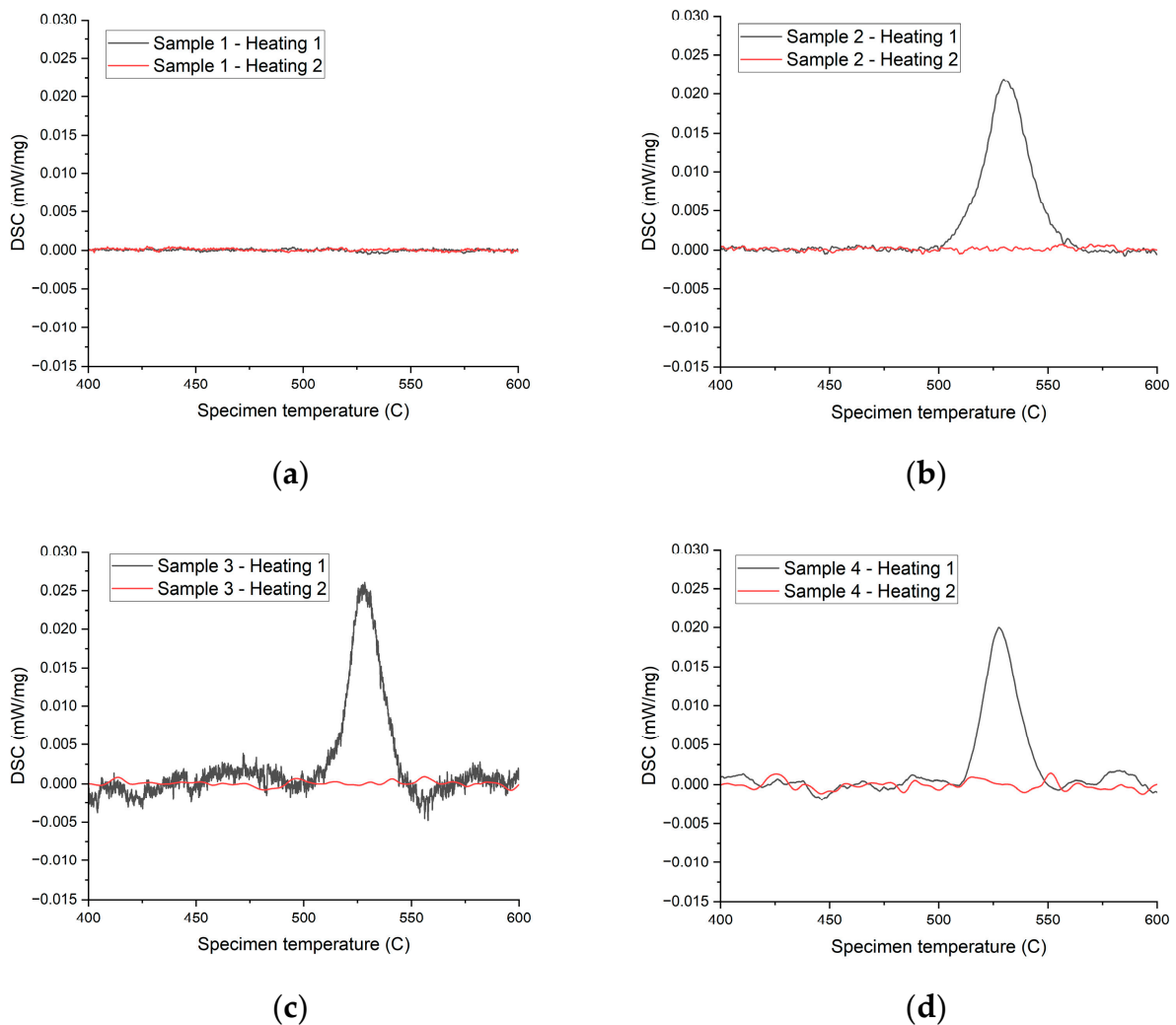


Figure 6. Differential scanning calorimetry curves of the primary and secondary heating of samples 1–4 (a–d).

Table 3. Onset temperatures and crystallization enthalpies of the 1CP matrix.

Sample	Onset Temperature, °C	Crystallization Enthalpy (J/g)
1	-	0.00
2	490	1.38
3	490	1.75
4	490	0.85

Differential scanning calorimetry data testifies that the 1CP matrix of the sample 3 have the highest amorphization degree among obtained samples. The initial 1CP powder is not fully amorphous and for that reason exact amorphization degree value of the samples cannot be determined [1]. Comparison of the crystallization enthalpies of sample 1 made of 1CP with sample 2 made of 1CP and Cu mixture with the same SLM parameters shows that addition of Cu allowed to significantly increase an amount of the amorphous phase in 1CP matrix, which proves the validity of the hypothesis about the impact of secondary material on composite matrix cooling. Lowered relative to sample 3 crystallization enthalpy of the sample's 2 matrix is conditioned by the low volume energy density, which relates to high hatch distance parameter and led to a decrease in cooling rate of the melt. Presence of heat retentive Cu also did not allow to put enough energy into the matrix. Speaking of sample 4, low hatch distance parameter value led to intense secondary heating, which

resulted in lower amorphous phase content. Comparison of the matrix crystallization enthalpy value differences allows to conclude that secondary heating has a stronger impact on amorphization of such composite matrix than a decrease in cooling rate of the melt.

Microstructure of the samples was examined with scanning electron microscope (Figure 7).

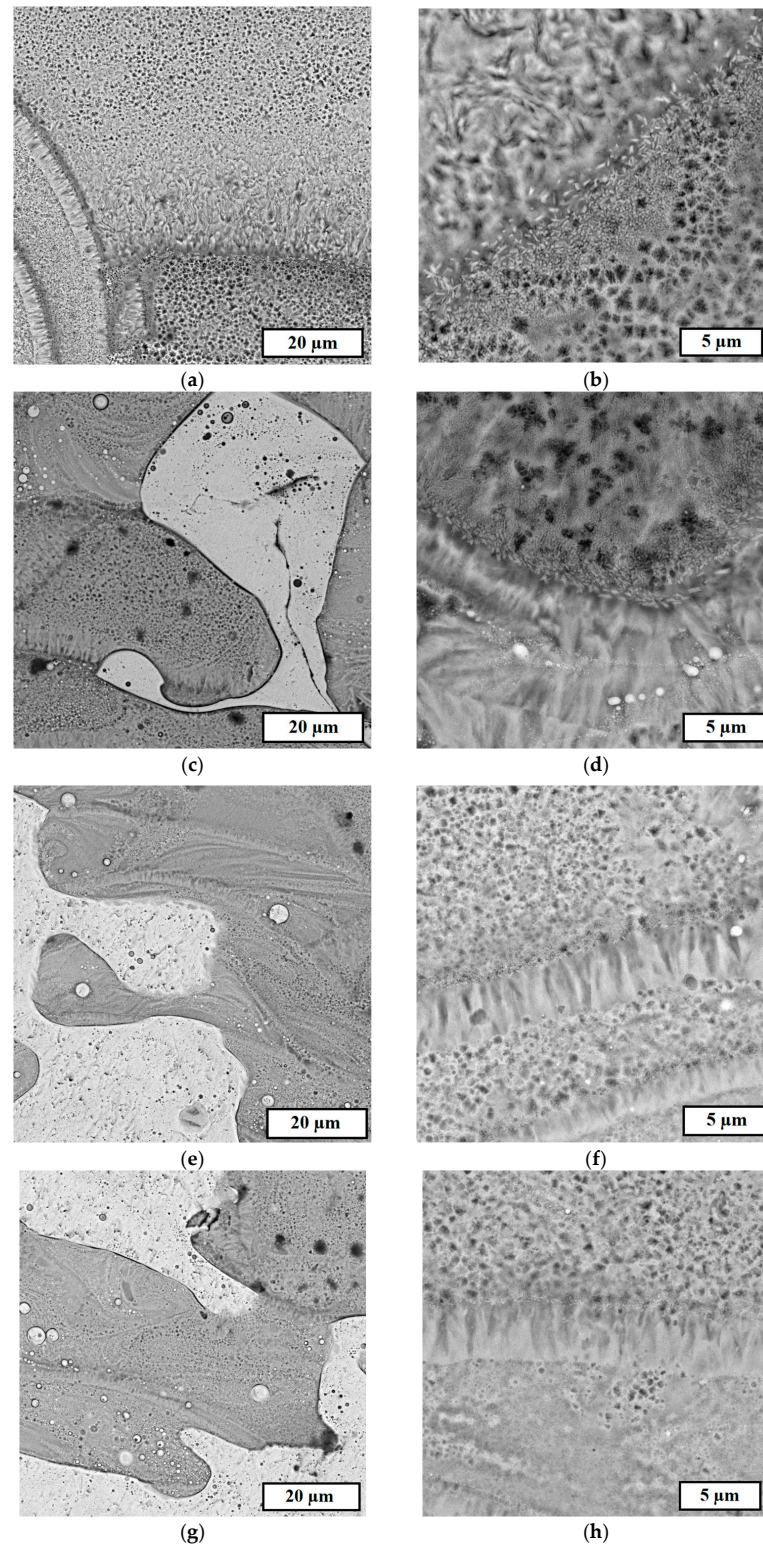


Figure 7. Scanning electron microscope (backscatter electrons mode) microstructure of the samples 1 (a,b), 2 (c,d), 3 (e,f) and 4 (g,h).

There are no major differences between 1CP and 1CP with Cu microstructure except Cu phase (light regions). 1CP microstructure consists of α -Fe solution matrix, Fe_2B precipitations (light polygons), located at the melting boundaries, and Fe_3Si ordered solid solution typical for alloys of such element system and indistinguishable for X-ray diffraction due to the similarity of the lattices of that and α -Fe solid solution (etching cavities). Energy-dispersive X-ray analysis of the surfaces showed that there was no significant diffusion of Cu into 1CP during the selective laser melting process (Figures 8 and 9).

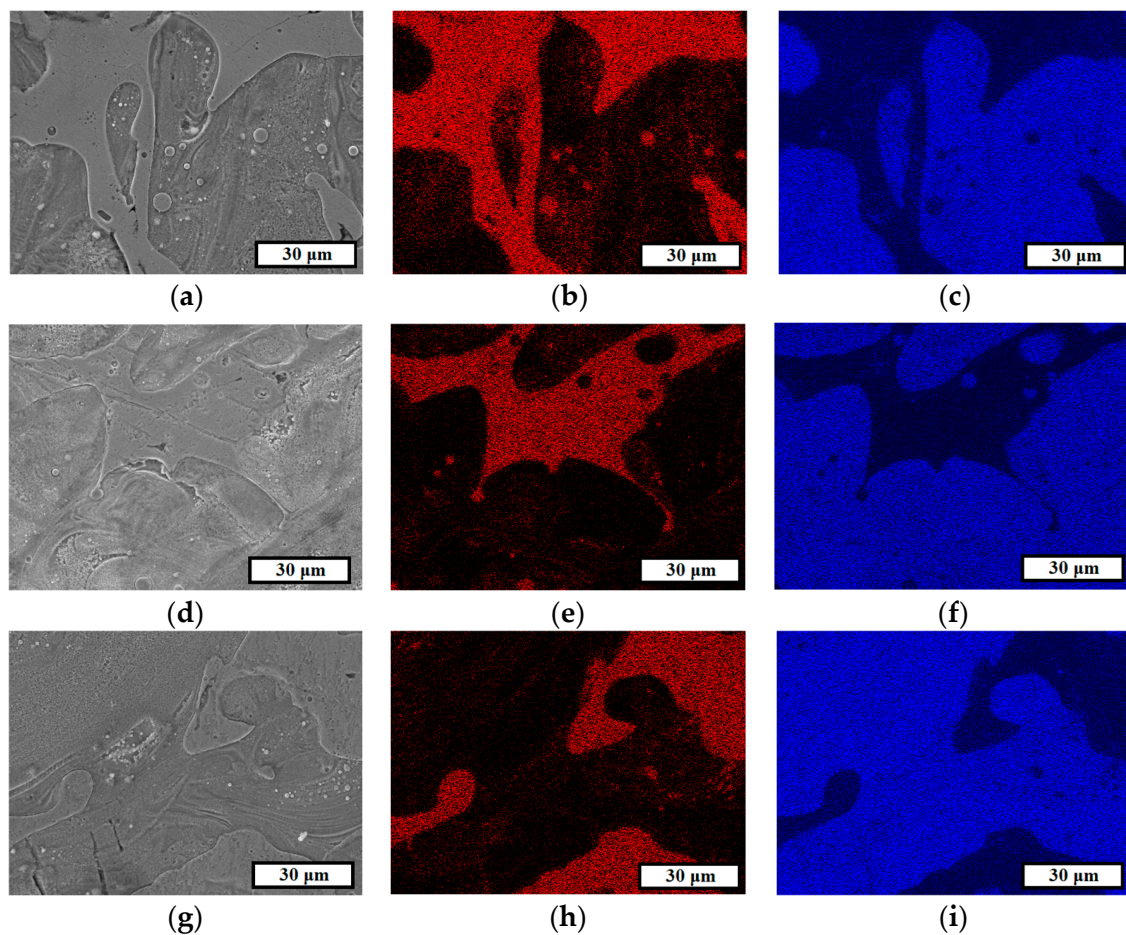


Figure 8. Results of energy-dispersive X-ray surface analysis of Fe and Cu for samples with Cu: analysis regions of samples 2, 3 and 4 (a,d,g), red Cu regions of samples 2, 3, and 4 (b,e,h), blue Fe regions of samples 2, 3, and 4 (c,f,i).

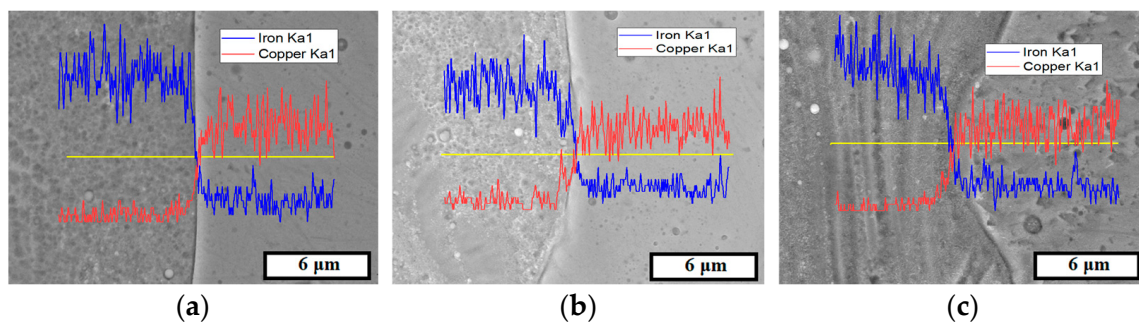


Figure 9. Linear energy-dispersive X-ray analysis of Fe and Cu results for samples 2–4 (a–c).

Energy-dispersive X-ray analysis along a line (Figure 9) shows that the depth of diffusion (of Cu in 1CP) zone is approximately 1 μm . Boundaries between the matrix and Cu show an absence of cracks, which indicates good wettability between 1CP and Cu.

Magnetic hysteresis curves of the samples are presented in Figure 10, magnetic properties numerical data are presented in Table 4.

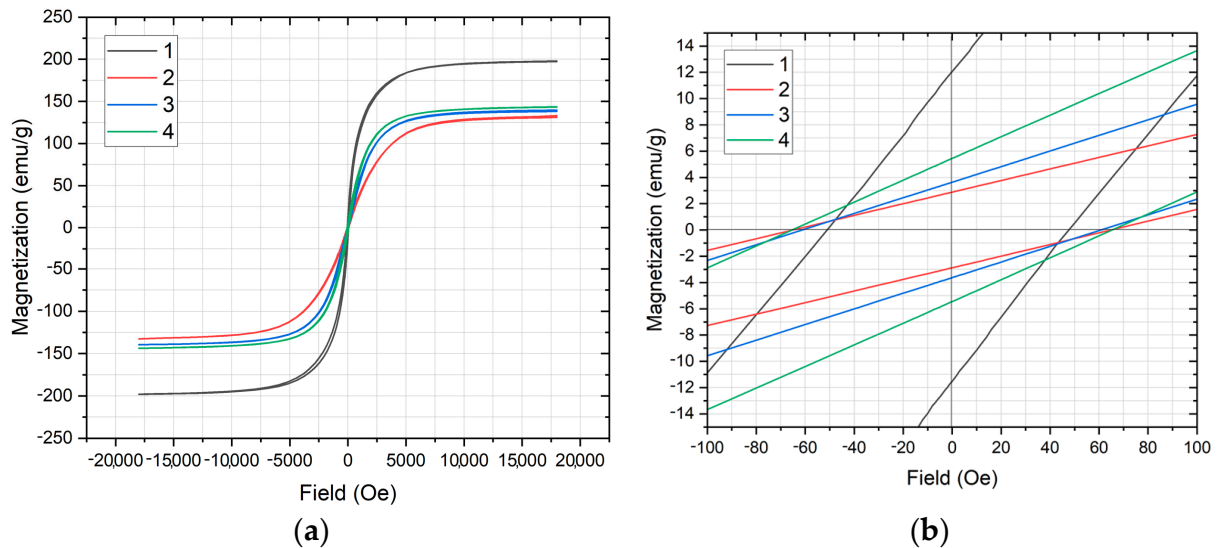


Figure 10. Magnetic hysteresis curves of the obtained samples: (a) general view of hysteresis loops; (b) enlarged area for coercivity estimation.

Table 4. Magnetic properties of the samples.

Sample	Coercivity (Oe)	Saturation Magnetization (emu/g)	Hysteresis Loop Area $\times 10^{-6}$ (Oe \times emu/g)
1	51	193.5	0.0870
2	66	132.6	0.0218
3	61	135.0	0.0272
4	65	139.5	0.0284

It is clear that magnetic properties of pure 1CP sample differs from that of composite samples: coercivity value is lower, saturation magnetization and residual magnetization values are higher than that of composite samples, which is connected with non-magnetic nature of Cu. Speaking of the composite samples, sample 3 has the smallest coercivity value which can be related to its relatively high amorphous phase content and density. Other composite samples showed almost equal coercivity values. Saturation magnetization values of all composite samples also does not differ significantly. Hysteresis loop area was calculated for all the samples to estimate the magnetic energy losses and it was found that sample 2 has minimal loop area (four times lower than that of pure 1CP sample 1 obtained with the same selective laser melting parameters). Difference between magnetic field energy losses of pure 1CP sample and composite sample is conditioned by zero amorphization degree and very high porosity level of pure 1CP sample. However, less porous composite samples demonstrate higher magnetic field energy losses relatively to sample 2. This fact indicates that pores clusters distributed in sample's volume may have a positive impact on the magnetic properties if their concentration is not too high. Positive effect of differently distributed hollows with defined geometry on magnetic field energy losses was investigated in [28] and since porosity level and pores clusters distribution are the most significant differences between structures of sample 2 and other composite samples, it can be assumed that such porous structure led to minimal magnetic energy loss of sample 2.

Chain of pores clusters can perform the role of dielectric layer which presence lowers the eddy currents contribution to core losses and this circumstance leads to reduction of core losses if remagnetization losses are equal. Porosity percentages of other composite samples (3 and 4) are much lower than that of sample 2 and such concentrations of loose spots in material's volume cannot allow to form a layer-like distribution of dielectric, hence, increase in porosity percentage in low porosity levels is detrimental on core losses by increasing the remagnetization losses, which allows to conclude that lower porosity percentage and higher amorphization degree of sample 3 explain its lower core losses relatively to sample 4.

The future direction of our work involves research of composite with different content of Cu, experiments with addition of other elements, deeper selective laser melting parameters investigation, and application of different scanning strategies. Combining the presented approach of element powder addition with the advanced scanning strategy may give better results by mutually reinforcing the positive effects of both approaches.

4. Conclusions

1. Addition of 10 wt.% of Cu in 1CP allows to halve the porosity percentage of selective laser-melted sample and minimize the cracks. Decreasing the hatch distance parameter from 0.12 mm to 0.08 mm allows to reduce the porosity percentage of the composite obtained with presented selective laser melting regime by 68%, but further decreasing hatch distance parameter to 0.05 mm results in slightly higher porosity relatively to sample with $h = 0.08$ mm, which is connected to recoating defects. Distribution of the Cu phase can be recognized as uniform in all composite samples, but in samples with 0.12 mm and 0.08 mm of hatch distance, Cu phase is presented in form of quasi continuous net, which cannot be said about sample with 0.05 mm of hatch distance, in which continuity of the Cu phase net is broken.
2. Phase composition of the composite samples is similar to that of pure 1CP sample (except for the presence of crystalline copper in composite samples) and is characterized by the presence of α -Fe solid solution and iron boride Fe_2B , which were revealed by X-ray diffraction, and also ordered solid solution Fe_3Si , which was revealed with scanning electron microscope.
3. Differential scanning calorimetry data showed that all the composite samples contain amorphous phase, which cannot be said about completely crystalline pure 1CP sample. Sample with hatch distance of 0.08 mm contain maximal amount of amorphous phase among the composite samples.
4. All the samples are characterized by the similar microstructure: Cu phase regions (absent for pure 1CP sample) and α -Fe regions with Fe_3Si solution distributed and Fe_2B locating at the melting lines. Wettability of Cu regions is decent as evidenced by the absence of cracks on the boundaries between the matrix and Cu. Energy-dispersive analysis showed that depth of diffusion (of Cu in 1CP) zone is approximately 1 μm in all the composite samples.
5. Comparison of the magnetic properties of the pure 1CP sample with that of composite sample obtained using same selective laser melting parameters showed that coercivity is 30% higher and saturation magnetization is 31% lower for composite sample, which is connected to the presence of non-magnetic material in sample's volume. However, magnetic field energy loss is four times lower for composite sample which is related to higher amorphization degree and optimal distribution and concentration of pores which can be considered as eddy current suppressing dielectric.

Author Contributions: Conceptualization, V.S.; methodology, V.S. and D.E.; formal analysis, D.E.; investigation, V.S. and D.E.; resources, V.S. and A.P.; data curation, D.E.; writing—original draft preparation, D.E.; writing—review and editing, V.S. and D.E.; visualization, D.E.; supervision, V.S. and A.P.; project administration, V.S.; funding acquisition, V.S. All authors have read and agreed to the published version of the manuscript.

Funding: The research was supported by a grant from the Russian Science Foundation № 21-73-10008, <https://rscf.ru/project/21-73-10008/> (accessed on 17 January 2023).

Data Availability Statement: Not applicable.

Conflicts of Interest: The authors declare no conflict of interest.

References

1. Sufiiarov, V.; Erutin, D.; Kantyukov, A.; Borisov, E.; Popovich, A.; Nazarov, D. Structure, Mechanical and Magnetic Properties of Selective Laser Melted Fe-Si-B Alloy. *Materials* **2022**, *15*, 4121. [[CrossRef](#)]
2. Erutin, D.; Borisov, E.; Popovich, A.; Sufiiarov, V. Magnetic anisotropy of a selective laser melted Fe-Si-B alloy. *J. Phys. Conf. Ser.* **2022**, *2361*, 012011. [[CrossRef](#)]
3. Schroers, J.; Paton, N. Amorphous metal alloys form like plastics. *Adv. Mater. Process.* **2006**, *164*, 61–63.
4. Schroers, J. Processing of bulk metallic glass. *Adv. Mater.* **2010**, *22*, 1566–1597. [[CrossRef](#)] [[PubMed](#)]
5. Kumar, G.; Tang, H.X.; Schroers, J. Nanomoulding with amorphous metals. *Nature* **2009**, *457*, 868–872. [[CrossRef](#)]
6. Li, N.; Li, D.J.; Wang, X.Y.; Liu, L. Size-dependent flowing characteristics of a Zr-based bulk metallic glass in the supercooled liquid region. *J. Alloys Compd.* **2012**, *523*, 146–150. [[CrossRef](#)]
7. He, J.J.; Li, N.; Tang, N.; Wang, X.Y.; Zhang, C.; Liu, L. The precision replication of a microchannel mould by hot-embossing a Zr-based bulk metallic glass. *Intermetallics* **2012**, *21*, 50–55. [[CrossRef](#)]
8. Xia, T.; Li, N.; Wu, Y.; Liu, L. Patterned superhydrophobic surface based on Pd-based metallic glass. *Appl. Phys. Lett.* **2012**, *101*. [[CrossRef](#)]
9. Li, N.; Xia, T.; Heng, L.P.; Liu, L. Superhydrophobic Zr-based metallic glass surface with high adhesive force. *Appl. Phys. Lett.* **2013**, *102*. [[CrossRef](#)]
10. Chen, W.; Liu, Z.; Robinson, H.M.; Schroers, J. Flaw tolerance vs. performance: A tradeoff in metallic glass cellular structures. *Acta Mater.* **2014**, *73*, 259–274. [[CrossRef](#)]
11. Liu, Z.; Chen, W.; Carstensen, J.; Ketkaew, J.; Mota, R.M.O.; Guest, J.K.; Schroers, J. 3D metallic glass cellular structures. *Acta Mater.* **2016**, *105*, 35–43. [[CrossRef](#)]
12. Li, N.; Li, D.J.; Liu, L. Correlation between flow characteristics and interfacial friction behaviour of a Zr-based metallic glass during micro-extrusion. *Philos. Mag.* **2013**, *93*, 1859–1872. [[CrossRef](#)]
13. Barrionuevo, G.O.; Ramos-Grez, J.A.; Walczak, M.; Sánchez-Sánchez, X.; Guerra, C.; Debut, A.; Haro, E. Microstructure simulation and experimental evaluation of the anisotropy of 316 L stainless steel manufactured by laser powder bed fusion. *Rapid Prototyp. J.* **2022**. Available online: <https://www.emerald.com/insight/content/doi/10.1108/RPJ-04-2022-0127/full/html> (accessed on 17 February 2023). [[CrossRef](#)]
14. Ravalji, J.M.; Raval, S.J. Review of quality issues and mitigation strategies for metal powder bed fusion. *Rapid Prototyp. J.* **2022**. [[CrossRef](#)]
15. Khorasani, M.; Ghasemi, A.H.; Leary, M.; Sharabian, E.; Cordova, L.; Gibson, I.; Downing, D.; Bateman, S.; Brandt, M.; Rolfe, B. The effect of absorption ratio on melt pool features in laser-based powder bed fusion of IN718. *Opt. Laser Technol.* **2022**, *153*, 108263. [[CrossRef](#)]
16. Safia, A.; Rima, D.; Nouredine, F. Effect of the Laser Scan Rate on the Microstructure, Magnetic Properties, and Microhardness of Selective Laser-Melted FeSiB. *J. Supercond. Nov. Magn.* **2018**, *31*, 3565–3567.
17. Nam, Y.G.; Koo, B.; Chang, M.S.; Yang, S.; Yu, J.; Park, Y.H.; Jeong, J.W. Selective laser melting vitrification of amorphous soft magnetic alloys with help of double-scanning-induced compositional homogeneity. *Mater. Lett.* **2020**, *261*, 1–4. [[CrossRef](#)]
18. Zou, Y.M.; Wu, Y.S.; Li, K.F.; Tan, C.L.; Qiu, Z.G.; Zeng, D.C. Selective laser melting of crack-free Fe-based bulk metallic glass via chessboard scanning strategy. *Mater. Lett.* **2020**, *272*, 127824. [[CrossRef](#)]
19. Jiang, Q.; Zhang, P.; Tan, J.; Yu, Z.; Tian, Y.; Ma, S.; Wu, D. Influence of the microstructure on mechanical properties of SLM additive manufacturing Fe-based bulk metallic glasses. *J. Alloys Compd.* **2021**, *894*, 162525. [[CrossRef](#)]
20. Jung, H.Y.; Choi, S.J.; Prashanth, K.G.; Stoica, M.; Scudino, S.; Yi, S.; Uta, K.; Kim, D.H.; Kim, K.B.; Jürgen, E. Fabrication of Fe-based bulk metallic glass by selective laser melting: A parameter study. *Mater. Des.* **2015**, *86*, 703–708. [[CrossRef](#)]
21. Żrodowski, Ł.; Wysocki, B.; Wróblewski, R. New approach to amorphization of alloys with low glass forming ability via selective laser melting. *J. Alloys Compd.* **2019**, *771*, 769–776. [[CrossRef](#)]
22. Zou, Y.; Qiu, Z.; Tan, C.; Wu, Y.; Li, K.; Zeng, D. Microstructure and mechanical properties of Fe-based bulk metallic glass composites fabricated by selective laser melting. *J. Non-Cryst. Solids* **2020**, *538*, 120046. [[CrossRef](#)]
23. Li, N.; Zhang, J.; Xing, W.; Ouyang, D.; Liu, L. 3D printing of Fe-based bulk metallic glass composites with combined high strength and fracture toughness. *Mater. Des.* **2018**, *143*, 285–296. [[CrossRef](#)]
24. Yang, D.; Liu, H.; Jiang, Q.; Jiang, Y.; Wang, X.; Yang, W. Atomic-level understanding of weakening crystallization in additive manufactured ternary Fe-based metallic glasses with Ni addition. *J. Non-Cryst. Solids* **2022**, *582*, 121435. [[CrossRef](#)]
25. Golod, V.M.; Sufiiarov, V.S. The evolution of structural and chemical heterogeneity during rapid solidification at gas atomization. *IOP Conf. Ser. Mater. Sci. Eng.* **2017**, *192*, 012009. [[CrossRef](#)]
26. Leung, C.L.A.; Marussi, S.; Towrie, M.; Atwood, R.C.; Withers, P.J.; Lee, P.D. The effect of powder oxidation on defect formation in laser additive manufacturing. *Acta Mater.* **2019**, *166*, 294–305. [[CrossRef](#)]

27. Drablia, R.; Alleg, S.; Fenineche, N.-E.; Escoda, L.; Suñol, J.-J.; Greneche, J.-M. Structure, Microstructure, Hyperfine, Mechanical and Magnetic Behavior of Selective Laser Melted Fe_{92.4}Si_{3.1}B_{4.5} Alloy. *Metals* **2022**, *12*, 1620. [[CrossRef](#)]
28. Goll, D.; Schuller, D.; Martinek, G.; Kunert, T.; Schurr, J.; Sinz, C.; Schubert, T.; Bernthaler, T.; Riegel, H.; Schneider, G. Additive manufacturing of soft magnetic materials and components. *Addit. Manuf.* **2019**, *27*, 428–439. [[CrossRef](#)]

Disclaimer/Publisher's Note: The statements, opinions and data contained in all publications are solely those of the individual author(s) and contributor(s) and not of MDPI and/or the editor(s). MDPI and/or the editor(s) disclaim responsibility for any injury to people or property resulting from any ideas, methods, instructions or products referred to in the content.